Sci. Technol. Arts Res. J., Jan.-March 2023, 12(1), 33-51
DOI: https://doi.org/10.20372/star.v12i1.03
ISSN: 2226-7522 (Print) and 2305-3372 (Online)
Science, Technology and Arts Research Journal
Sci. Technol. Arts Res. J., Jan.-March 2023, 12(1), 33-51
Journal Homepage: https://journals.wgu.edu.et

Original Research

Delineation of Gold mineralization zones using Induced Polarization and Magnetic Methods at Adare Green Stone Belt, Nejo, Oromia, Ethiopia

Hailu Getachew & Fekadu Tamiru*

Department of Earth Sciences, Wollega University, P. O. Box: 395, Nekemte, Ethiopia

Abstract

This study looked at potential gold mineralization in the Adere green stone belt in the Nejo district and used magnetic and induced polarization techniques to identify mineralized zones. Utilising magnetic and induced polarization techniques, thirteen profiles were examined to pinpoint the location of the gold deposit. Accordingly, the alteration zones were connected with anomalous zones of gold mineralization that had medium to high chargeability and high resistivity. The chargeability anomalies are primarily related to metallic sulphide mineralization and are induced by sulphide manifestations that suggest potential locations for gold resources. First, the tilt derivative maps, followed by the vertical derivative maps, show the various trending aspects on the analytical signal. High contact zones are visible at shallow depths. The quartz veins were intimately related to gold mineralization and are primarily located in migmatites. In general, every line section describes a high chargeability attribute. These zones may result from diffused sulphide mineralization in silicified strata; these minerals may be associated with valuable minerals found in gold occurrences. High chargeability anomalies that stretched beyond 60 m were visible in the inverted chargeability and resistivity sections.

Article Information

Article History:
Received : 08-01-2023
Revised : 25-02-2023
Accepted : 26-03-2023

Keywords:
Gold Mineralization, 2D model, Chargeability, Resistivity, Anomalies

*Corresponding Author:
Fekadu Tamiru

E-mail:
fekadugebissa@gmail.com

INTRODUCTION

Mineral and other natural resource resources abound in Ethiopia. According to Asrat (2001), the earliest rocks for these resource deposit occurrences in Ethiopia are late Proterozoic to Paleozoic metamorphic rocks formed by pan-African orogenic processes. These rocks result in medium- to high-grade schists and gneisses, as well as related granitic and mafic/ultramafic intrusions. Ethiopian geology forms the southern portion of the Arabian Nubian Shield (ANS) and dates back to the Precambrian (generally) and Neoproterozoic (exactly). Ethiopia's greenstone belts are recognised as extensions of the Arabian-Nubian shield, encircled by the Mozambique belt, a high-grade metamorphosed belt. In Ethiopia's green stone belts, low-grade metamorphosed volcano-sedimentary rocks are the main sources of gold. In contrast to the other gold belts in the nation, the main green stone belts of the western green stone belt are located in the western portion of Ethiopia. Thus, following different reports of exploration of gold and other expensive metals in large quantities, these regions have just attracted the attention of investors and researchers, though the gold potential of these areas is not completely evaluated.

Gold mining has mostly been extracted from placer deposits and, to a lesser extent, from primary free gold mineralizations. Geologically favourable areas have been known in the green

stone regions in the northern part of Ethiopia in Tigray, in the southwest portion of the Akobo river basin, in the south portion of Adola, Agremariam, Arero, and Moyale, and in the western part of the green stone rule that includes areas of Western Wollega and the Benishangul-Gumuz region. The main mineralizations contain oda godere, daletti, ondonok, kata, Adere, and Guba areas, some of which have been well-known for over a century in Ethiopia. Widely alluvial gold mining has been directed by external companies and the local people since a long time ago. However, in the exploration of mineral deposits, it is impossible to observe in detail every square kilometre of an area of geological structures that directly or indirectly proposes the existence of a given mineral deposit. The possibilities of surface geological and geochemical investigations have become less effective. The topographical, geological, and mineralogical information is considered to determine whether, if at all, geophysical methods should be used in the area, which would be most appropriate (Getaneh, 2007). Geophysical investigations of the subsurface earth require measurements at or nearest to the surface of the earth that are affected by the internal distribution of physical properties. Analysis of this measurement can reveal how the physical properties of the subsurface differ vertically and laterally**.** Thus, the geophysical method helps to get evidence about the subsurface over a substantial area in a reasonable time structure and in a cost-effective way (Sisay, 2008)**.**

Hence, induced polarisation (IP) and magnetic methods are the most effective geophysical methods to map the geological continuity of mineralization. Thus, it has extensive application to minerals to identify sulphide minerals and detect structures and lithology. The induced polarisation (IP) method is also used to map the economic sulphide deposits. Induced polarisation and magnetics are the geophysical methods used in this study for mapping and detecting the gold mineralization of the Adare Green Stone Belt of Nejo District in Oromia Regional State, Ethiopia.

Location and accessibility of the study area

The study was performed in the surrounding area of Nejo town in Oromia regional state, at a distance of about 7km on the east side of the town and located in geographical coordinates of 781750m to 782500m east and 1049250m to 1050500m north (Figure 1). The total area of the gold potential assessment coverage is about 0.84 m^2.

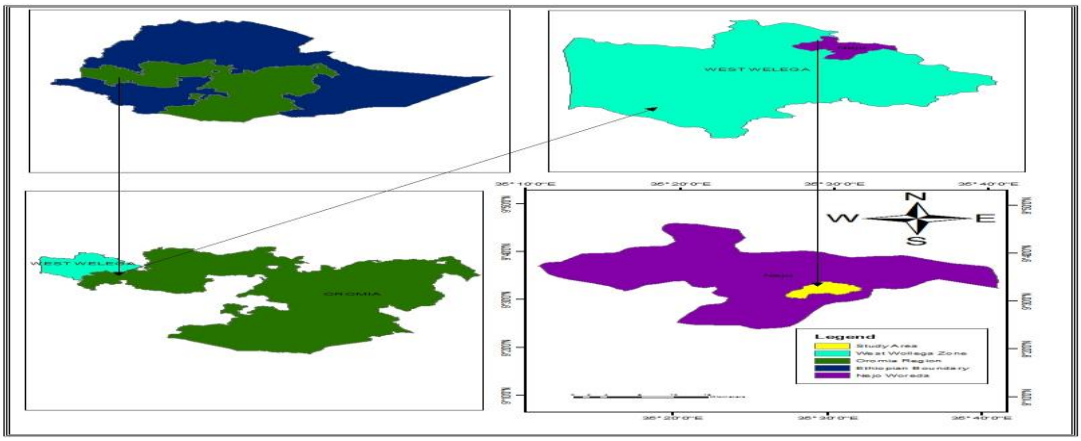

Figure 1 *Location map of the study area*

Geological setting of the study area

The Mozambique Belts (MB) and the Arabian Nubian Shield (ANS) are the two components of the Pan-African Orogeny. The geodynamics of the East African Orogeny can be understood primarily from these two terrains. Compared to other countries in the Horn of Africa, Ethiopia is reported to have more projected out crops

(Kazmin, 1972; Berhe, 1990; Asrat, 2003). Ethiopia's precambrian landscape holds a special place on the African continent. Nejo District is situated in the western Wollega zone of the Oromia region, which is part of the western Ethiopian precamberian topography. The region is composed of high grade gneissic and migmatite assemblages sandwiched between low grade volcanic and sedimentary rock collections. This contact shield is found in the Arabian-Nubian Shield's juvenile Neoproterozoic crust, primarily in the gneissic Mozambique Belt (Yada, 2017).

REGIONAL GEOLOGY

Rocks that are plutonic and supra-crustal comprise Western Ethiopia. There are two distinct portions to its Precambrian regions. To the east are these Achaean quartz field spathic gneisses, while to the west are various meta-volcanoes, meta-conglomerates, phyutes, quartzite, marbles, and metacherts. These are Proterozoic units. The younger Neoproterozoic crust of the Arabian Nubian Shield and the older, mostly gneissic Mozambique Belt include the Precambrian counterparts of the western Ethiopian shield (Woldemichael, 2010). The study location is located on Ethiopia's western basement rock, according to the regional geological context (Figure 2). Similar to the Mozambique Belt in the Pan-African East African orogen, and the Arabian Nubian Shield (ANS), the Western Ethiopian Shield (WES) is the greatest of the country's Precambrian coverings. Rocks that are plutonic and supra-crustal comprise Western Ethiopia. Its Precambrian provinces could be divided into two parts. Archean quartzo fielde sphatic gneisses in the east and Proterozoic units consist of various meta-volcanites, meta-conglomerates, phyutes, quartzites, marbles, and metacherts to the west.

Metasedmentary Rocks (Pams)

These rocks are found on the central and northern sides of the study area (Figure 2). Metasedmentary rock is gneiss, including rocks rich in quartz sericite phylite and Q-sericite schist and showing gneissis structure. Quartzites are found as a major intercalating unit within the area.

Massive medium-grain granite and alkaline pyroxene (Pgt3)

The northern portion of the study area is where this rock is located. The following are possible minor essential minerals found in granite: pyroxene, amphibole, biotite, and muscovite. The most prevalent plutonic rock in the Earth's crust, granite is an intrusive igneous rock with coarse or medium grains that is rich in quartz and feldspar. It is created when silicate melt, or magma, cools down below the surface.

Metamorphic and metasand stone (Pgl)

When rocks are exposed to extreme temperatures, high pressures, hot fluids rich in minerals, or, more frequently, any combination of these conditions, metamorphic rocks are formed. Although they began as a different kind of rock, metamorphic rocks have undergone significant alteration from their igneous, sedimentary, or previous metamorphic forms. Tectonic forces acting on sedimentary rock (sandstone) create metamorphic rocks. standing for: silt that was deposited in the Neoproterozoic Era It

encompasses the eastern and western regions of the research area.

Fine-medium-grained gabbro (Pgb)

Any of a number of medium- or coarse-grained rocks with a predominance of pyroxene and plagioclase feldspar is known as gabbro. In essence, gabbro is the intrusive (plutonic) counterpart of basalt; but, unlike basalt, which is frequently quite uniform in composition and mineralogy, gabbros exhibit a great deal of variability. It located itself in the north-western section of the research area.

Lower basalt (TLB)

It is situated at the study area's corner. Basalt is a dark-colored, extrusive igneous (volcanic) rock with a low silica content and a relatively high iron and magnesium content.

Coarse-grained Pyroxenite (PPxt)

Pyroxenite is an ultramafic igneous rock that is composed of minerals belonging to the pyroxene group, including enstatite, augite, diopside, hypersthene, and bronzite. This coarse-grained rock, which is found in the southeast of the research area, has at least 90% pyroxene minerals in it.

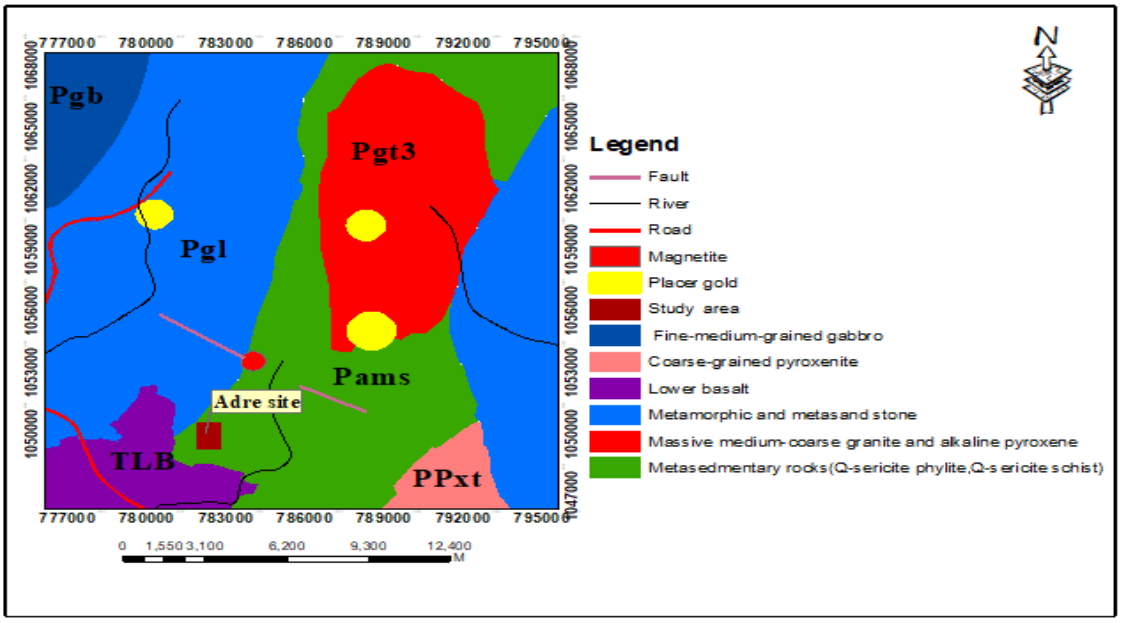

Figure 2 *Geological map of Adere area (Extracted from minerogenic prognosis map of Gimbi-Nejo area)*

Local Geology of the Area

Western Wollega is the most representative exposed pan African basement area in Ethiopia. Various pan African intrusive rocks and Volcanic together with Precambrian layers are wide spread. Nearly north south trending Baruda Tullu Dimtu Yubdo structural belt runs through the area. Based on different previous works, western Ethiopian shield is classified into four different domains; Katta domain, Chochi domain, Aba Sina domain and Afa domain (Yada, 2017). The main mineralization in the Kata, Adare, Gida

Maryam, Bushane Alaltu and the surrounding area includes, sheet swarms and stock works of gold-bearing quartz veins beginning at or near the surface. The fine to flaky gold associated with sulfides (pyrite, chalcopyrite), iron oxides, Cupper, garnet and epidotic minerals. Based on panning results, they concluded that the main economic potential of gold exists in the area as the type of gold mineralization, volcanogenic massive sulphides.

MATERIALS AND METHODS

In this study the induced polarization and magnetic methods geophysical techniques were employed.

Induced polarization survey method

The 4Point Light10HP frequency domain transmitter, which is powered by a motor generator, and the 4Point Light10HP receiver were used for chargeability and resistivity measurements. It is an eight-channel time domain receiver capable of receiving signals simultaneously from up to eight dipoles. It measures primary voltage (Vp), self-potential (SP), and time-domain induced polarisation (Ma) with periods varying from 1 to 32 seconds (Scintex, 993) and automatically calculates the average chargeability (Mx) and apparent resistivity (ρa) parameters. The measured readings were conducted in terms of electrical resistivity and chargeability in the time domain along thirteen profiles within 5m spacing between electrodes. The separation between each profile was about 100 m, where each profile has a length of 595m in a dipole-dipole arrangement. The layout of the profiles was based on prior structural design to be orthogonal in the veins and lode quartz recognized. In order to increase the depth of investigation, measurements were made with increasing values of n (n=1 = 1–5) and gradually increasing the distance between the transmitting and receiving electrodes. The inter-electrode spacing was 5 m, and the maximum separation of the dipole-dipole configuration was 5n, where n is a multiple of electrode separation. The current electrodes were shifted every few lines in order to get a good signal for recording the potential difference.

The data were inverted using the RES2DINV inversion software to produce a 2D model of chargeability and resistivity. The inversion of induced polarisation data is conducted by the least-squares method involving finite-element and finite difference methods**.** The IP data is processed with the use of Oasis Montaj version 6.4.2 and Surfer Software version 10. Gradient data are presented in the form of maps, while dipole-dipole data are presented as pseudo-sections (Figure 4). Maps for dipole levels have been plotted to inspect lateral variations of chargeability and resistivity at different depths.

Magnetic Survey Method

The Proton Precision Magnetometer was used to measure the total magnetic field to a resolution of 0.1 nT with an accuracy of 0.5 nT. Before the survey measurement was conducted, a fixed base station for all profiles was established closer to the survey grid areas in order to control the daily variations of the earth's magnetic field. The data was collected along thirteen profiles, each covering a distance of 595 m, with having data spacing of 5m and a profile separation of about 100m. Additionally, magnetic data were also collected randomly within and at the boundary of the study area. The total magnetic anomaly obtained was processed to produce a total magnetic anomaly map, an analytical signal map, a first derivative map, and tilt derivative maps.

RESULTS AND DISCUSSION

Induced Polarization Survey

An induced polarisation survey is effective in detecting disseminated metallic sulphide mineralization zones, and resistivity maps can delineate structures as contacts, faults, shear, and

alteration zones, which could indicate possible mineralized areas.

Chargeability and Resistivity Maps

The chargeability and resistivity maps are given in Figures 3a and 3b. High chargeability greater than 12 mV/v and low resistivity less than 10Ω m responses in the central, western, and north-eastern areas indicate massively weathered graphite. High chargeability corresponds with high resistivity in the central south and north, indicating the area of massive sulphide minerals or metasegregary rocks that contain the sericite phylite and quartzite-Sericites chist and show the gneiss's structure. Quartzites are found as a major intercalating unit within the area around the contact with granite rocks and contain sulphide minerals. A patch of low chargeability less than 9 mV/v and high resistivity greater than 12Ω.m in the southwestern end and south eastern indicate the area of lime stone rock occurrence, whereas at the centre of west and central southeast, a striking low linear zone in the central area shows a fault zone. There is pyrite mineralization and graphite occurrence in this anomalous area, which could be causes for high chargeability zones. This map also shows the north, south, and east-west trending lines that are indicated in the chargeability map.

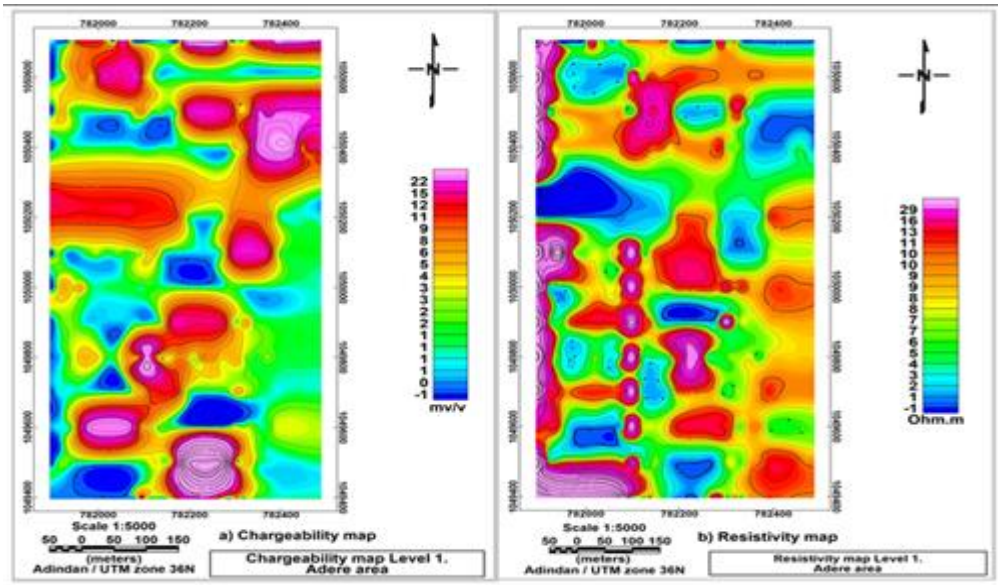

Figure 3 *a) Chargeability and b) Resistivity anomaly map*

Apparent chargeability and resistivity data were displayed in pseudo-section plots with topography for qualitative interpretation. Pseudo sections give an approximate picture of the subsurface geology, although the resulting images are artefacts of the plotting procedure. High chargeability features are delineated on all line sections, and the source of anomalies extends deeper beyond the detection limit of the electrode configuration used for this survey. High chargeability zones are not correlated with high resistivity.

Chargeability and resistivity pseudo-sections of lines 494N–504N are given in Figure 4. (a)-(f). On these lines, the chargeability anomaly is generally dipping west. The corresponding resistivity reveals high zones on the western side and low responses on the eastern part. Along all sections, chargeability bodies extend to depths beyond the detection limit of the electrode configuration used. Chargeability and high resistivity signatures do correspond.

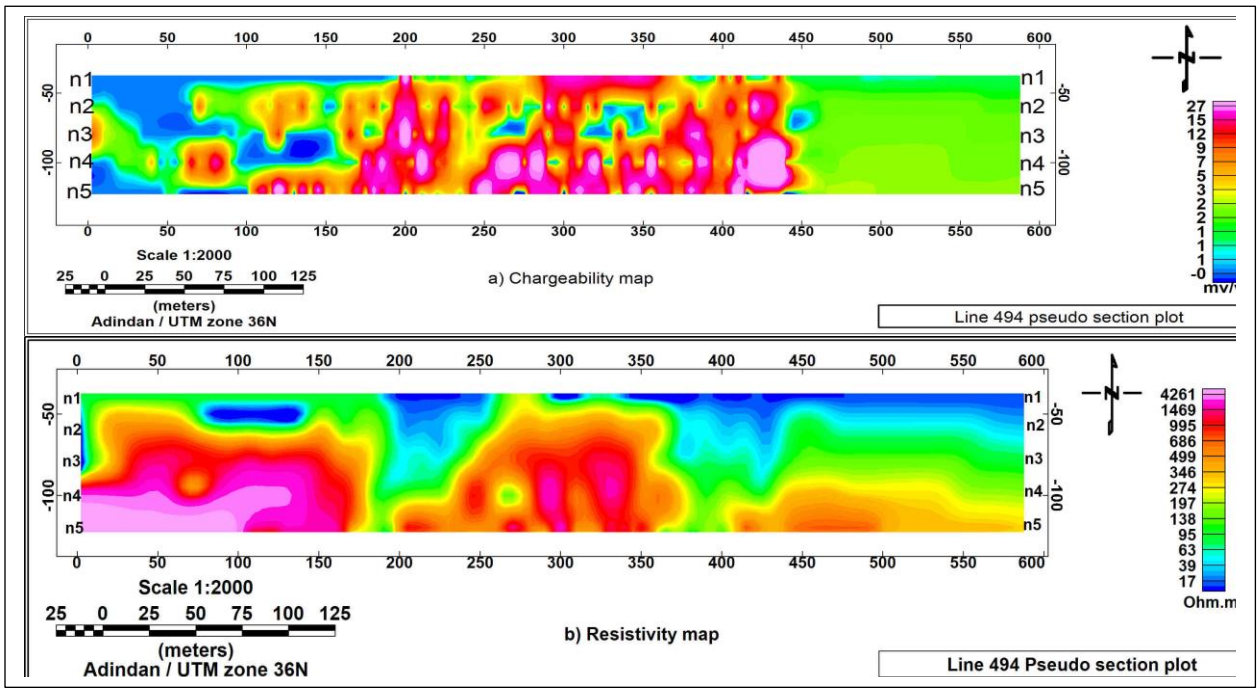

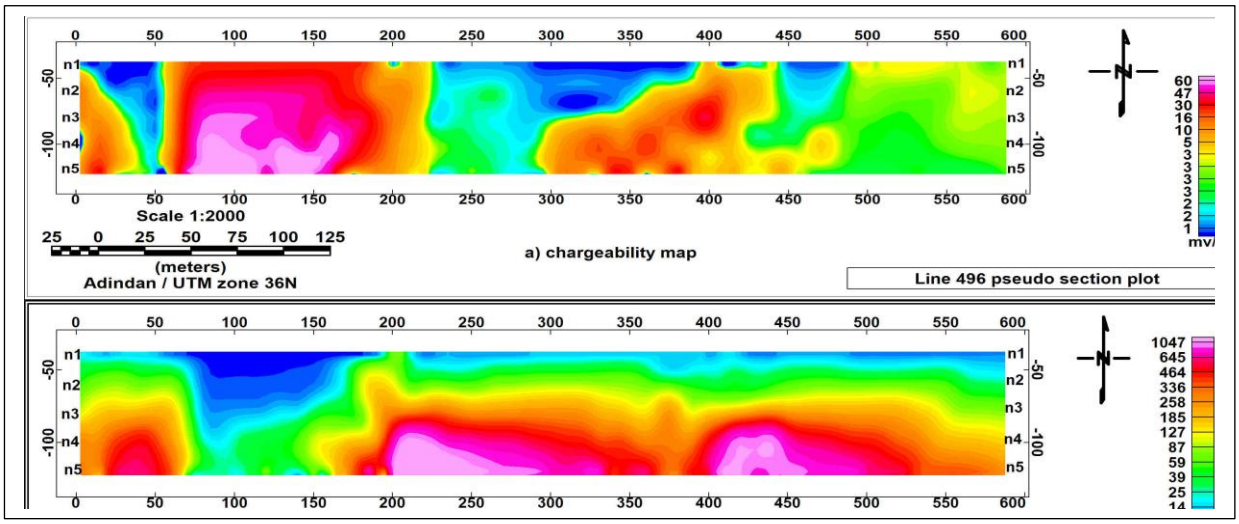

(b) Chargeability and Resistivity Pseudo section map of Line 496N.

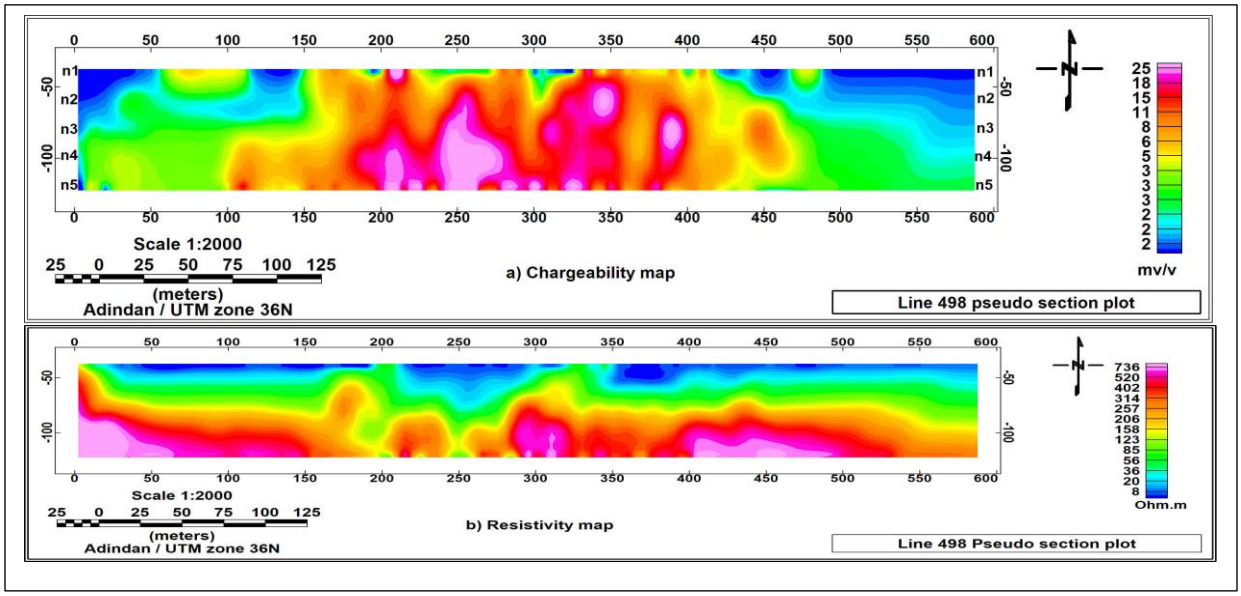

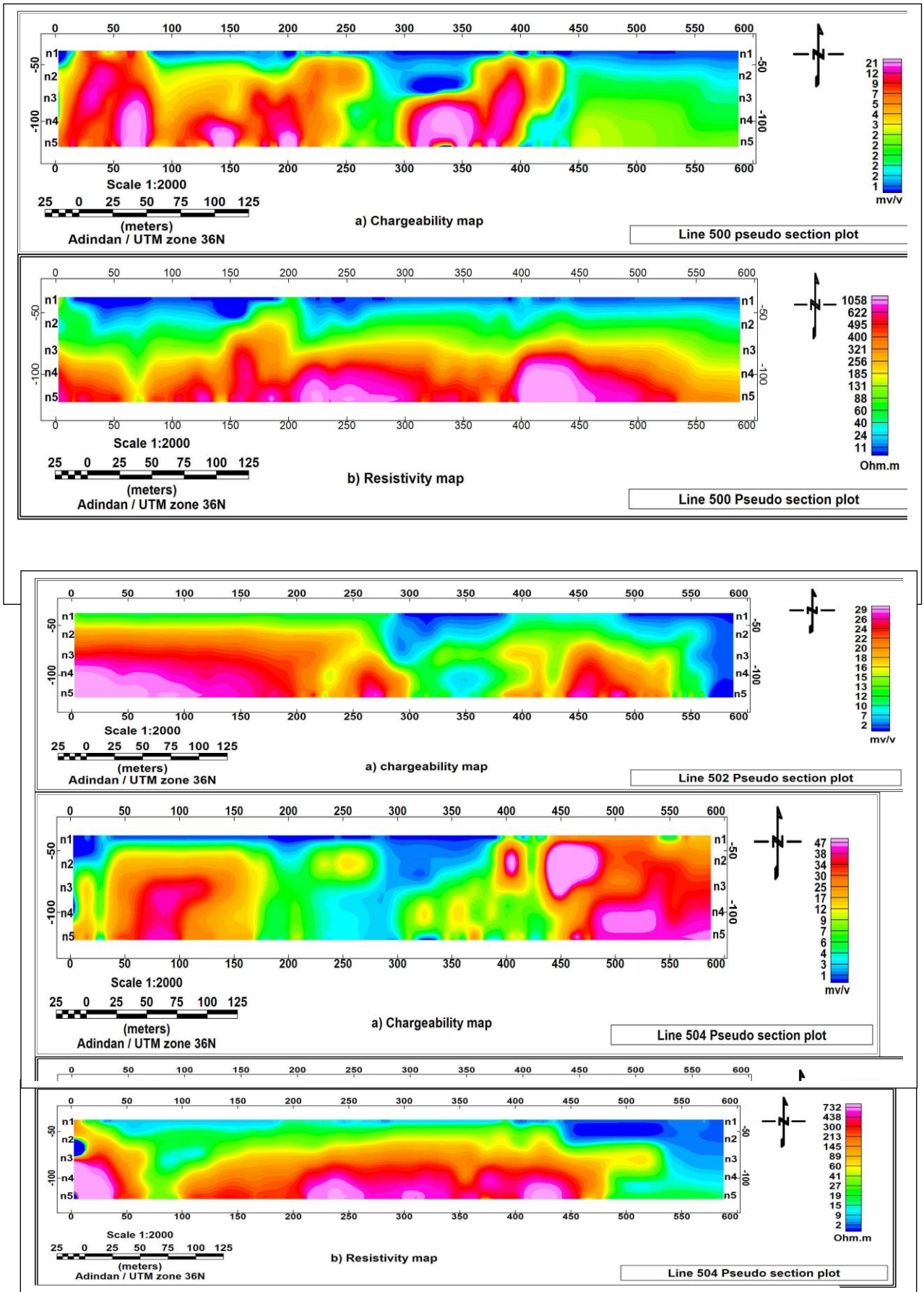

Figure 4. Chargeability and Resistivity Pseudo section map of Line 494N to Line 504N

Inverted Model of Electrical Resistivity Tomography and Chargeability Profiles

Chargeability and resistivity data were inverted using RES2DINV inversion software to produce 2D model of chargeability and resistivity distribution of the subsurface. The inversion was conducted by least-square method involving finite-element and Finite difference method (Geotomo software, 2015). The Model of inverted lines L494N, L496N, L498N, L500N, L502N, and L504N are given in Figure 5 to Figure 10. Figure 5 is the inversion section of Line 494N for 2D chargeability and electrical resistivity imaging. This profile covers the total length of 585m and contains 1431 chargeability and resistivity data points that were used for the inversion. The centre of the south and southeastern sides of the line is defined by high resistivity and medium chargeability. In the central part between 405m and 445m, high chargeability corresponding to low resistivity at depth is a peculiar feature. This peculiar anomaly may have been caused by graphite or pyrite occurrences.

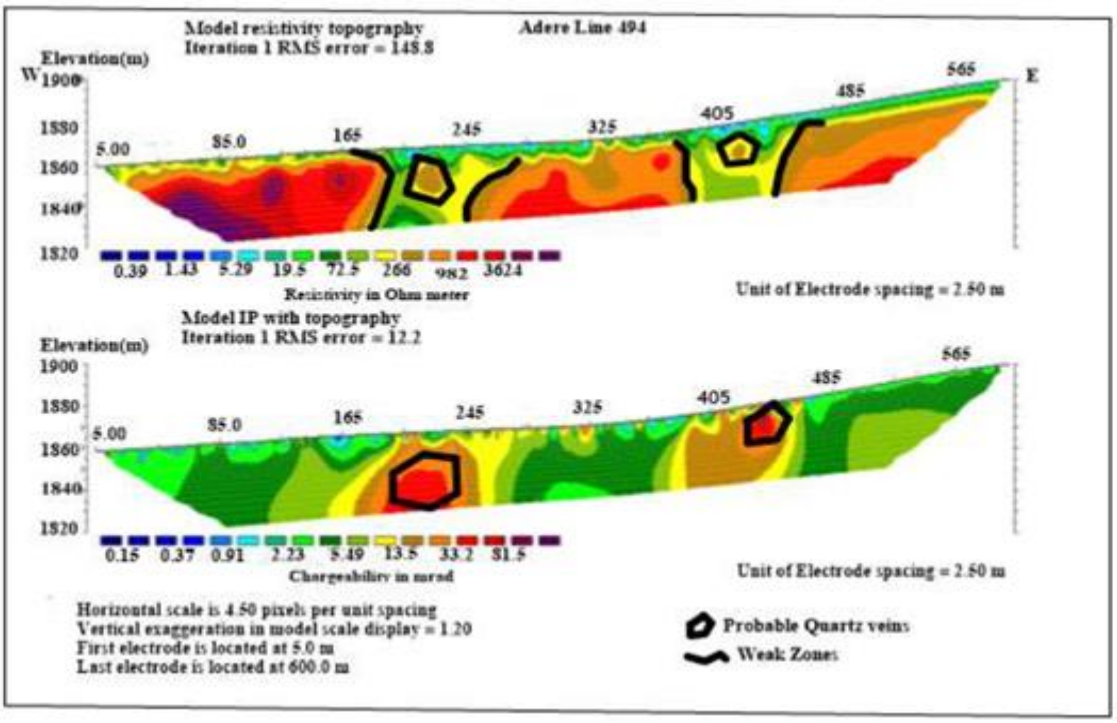

Figure 5 *Chargeability and 2D electrical resistivity imaging inverse model of line 494*

Inverted Model of Chargeability and Resistivity of Line 496N

In the inverted section of Line 496N (Figure 6), the southwestern and southeastern parts have moderately high resistivity and low chargeability. This profile covers a total length of 585 m, and the electrode location is 5m. The 1388 chargeability and resistivity data points were used for the inversion. The area between 85 and 205 has very high chargeability at the south and low resistivity at the northern part.

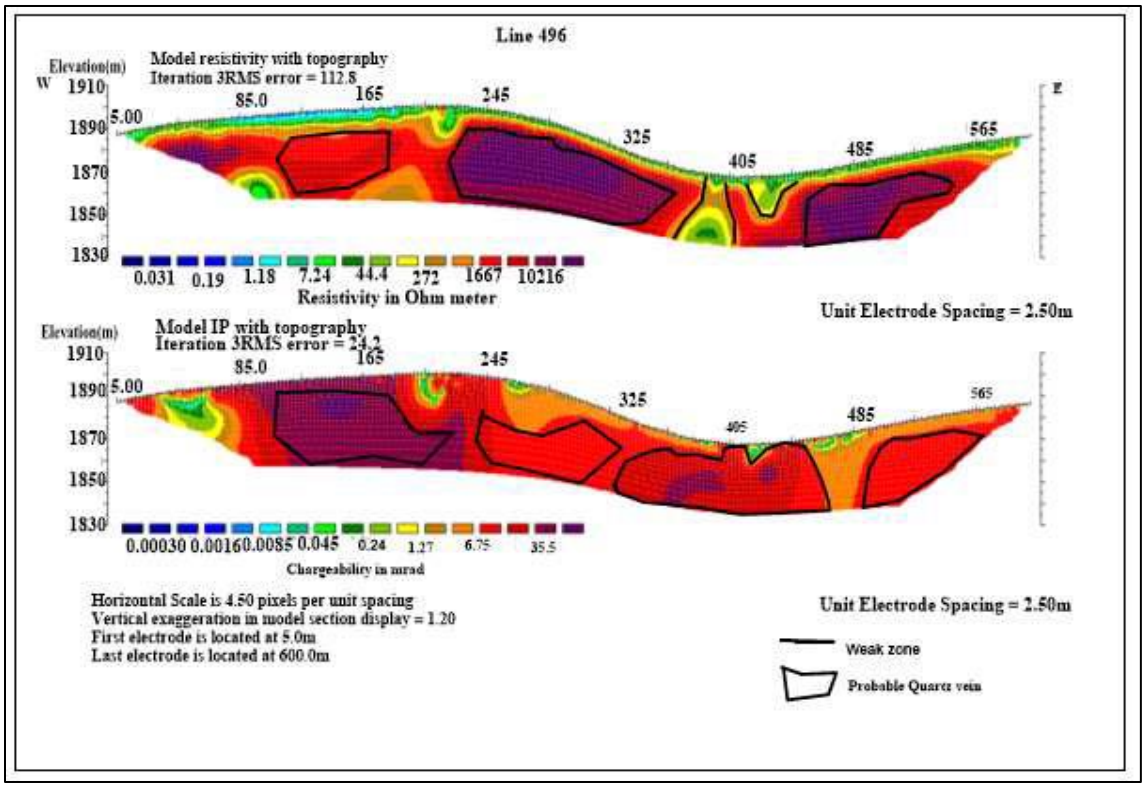

Figure 6 Chargeability and 2D electrical resistivity imaging inverse model of Line 496

Inverted Model of Chargeability and Resistivity of Line 498N

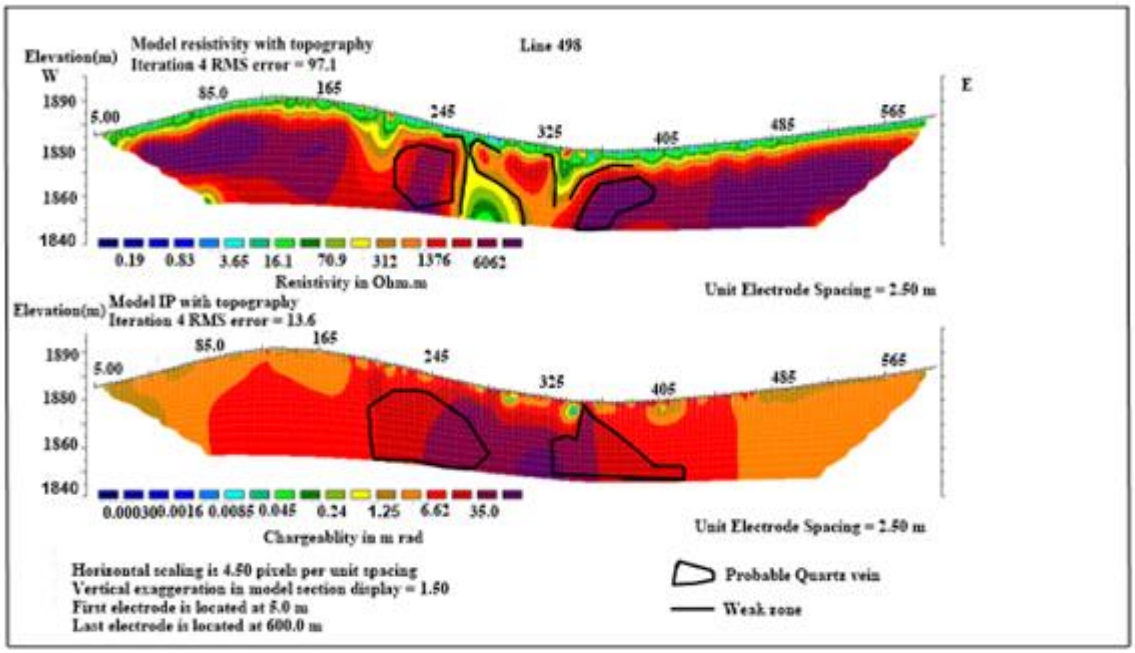

Figure 7 Chargeability and 2D electrical resistivity imaging inverse model of line 498N

From the Figure 7 inversion section of Line 498N, the central southern part of the area between 205 and 445 is defined by high chargeability and medium resistivity. The northern area of figure 4.9 has low resistivity and is medium between 245 and 365. This profile covers a total length of 585 m, and the electrode location is 5m. The 1480 chargeability and resistivity data points were used for the inversion.

Inverted Model of Chargeability and Resistivity of Line 500N

The inverted section of Line 500N (Figure 8) describes high chargeability around the southeast between 410 and 445 and low resistivity in the northern area, which could be due to highly weathered rocks. This profile covers a total length of 585 m, and the electrode location is 5m. The 1515 chargeability and resistivity data points were used for the inversion.

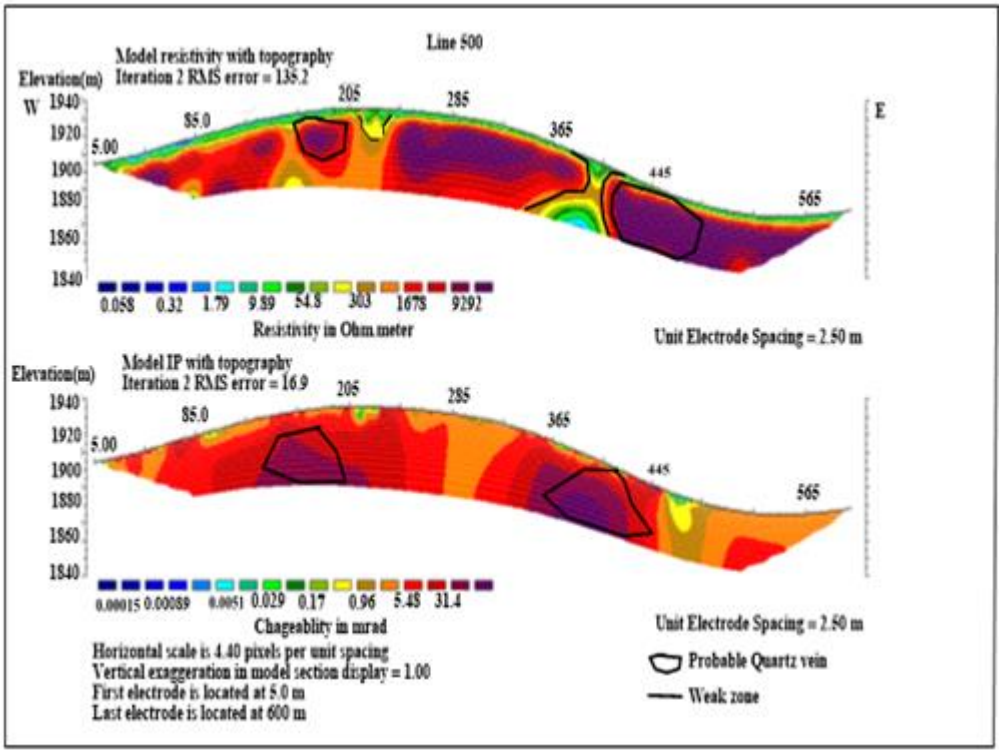

Figure 8 *Chargeability and 2Delectrical resistivity imaging inverse of model of Line 500N*

Inverted Model of Chargeability and Resistivity of Line 502N

Figure 9 is an inverted section of Line 502N. The southern part between 205 and 485 is defined by high resistivity, whereas the northwestern side has low to medium resistivity. The chargeability section of this line shows high chargeability at depth, possibly indicating graphitic or pyritic-type rock occurrence. This profile covers a total length of 585 m, and the electrode location is 5m. The 1476 chargeability and resistivity data points were used for the inversion.

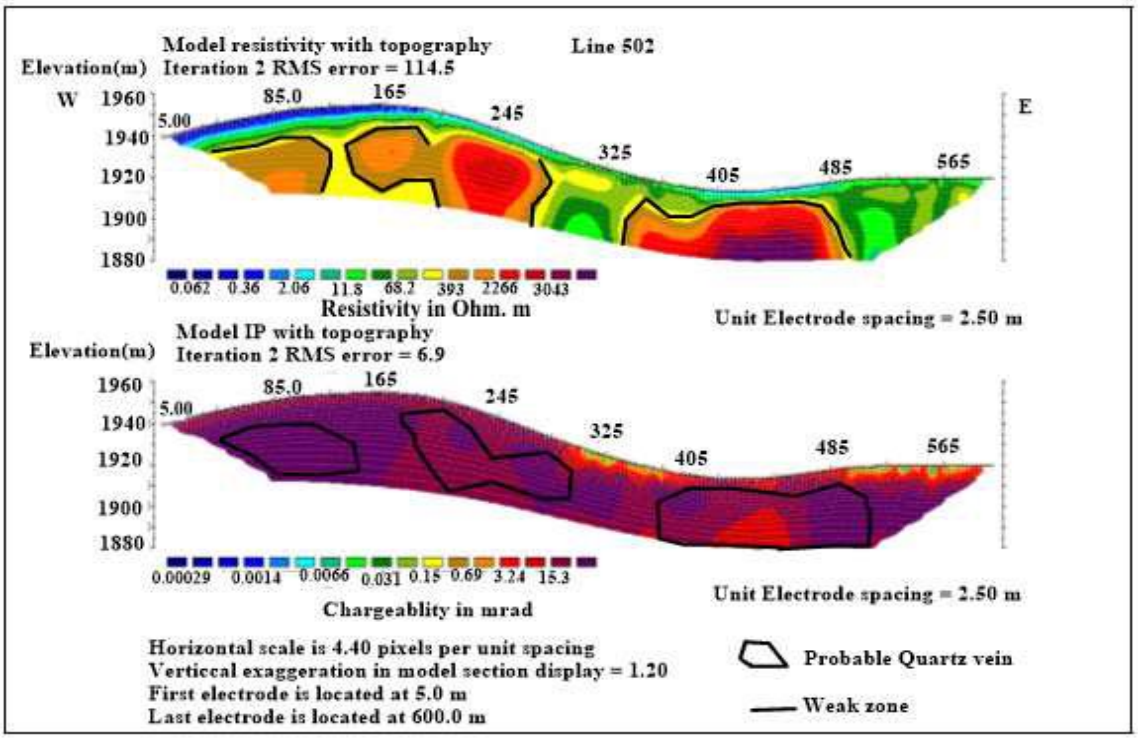

Figure 9 *Chargeability and 2Delectrical resistivity imaging inverse model of Line 502N*

Inverted Model of Chargeability and Resistivity of Line 504N

Figure 10 is an inverted section of Line 504N. The north part of the area has low resistivity and high resistivity at the centre of the southeast. The chargeability section of this line shows high chargeability in the middle of the south between 370 and 430, whereas the south-eastern area between 70 and 165 has medium chargeability. This profile covers a total length of 585 m, and the electrode location is 5m. The 1437 chargeability and resistivity data points were used for the inversion.

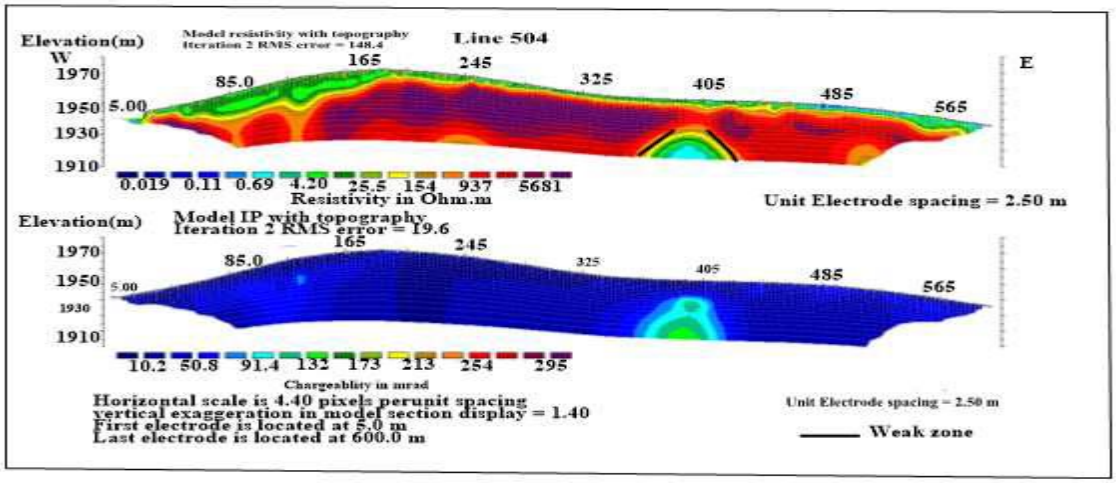

Figure 10 *Chargeability and 2Delectrical resistivity imaging inverse of model of Line 504N*

Resistivity and Chargeability Sliced Stacked Depth Maps

From the RES2DINV output, the resistivity and chargeability values for various depths were taken out and converted to the surfer format. To comprehend the whole geological framework, it is imperative to observe both the vertical and lateral variation of electrical resistivity and chargeability over the area from a synoptically oriented perspective. The resistivity and chargeability values obtained from the dipole-dipole configuration data collected on the profiles are easily obtained by looking at a sliced-stacked map. According to Yusefi, Hafizi, and Salari (2017), these 3D visualisation models aid in the comprehension of intricate geological systems during mineral prospecting.

The Stacked Resistivity Map Interpretation

In order to visualise the entire surveyed area in terms of the resistivity value distribution, the resistivity sliced-stacked depth map, or Figure 11, was created from the 2D electrical resistivity dipole-dipole array data of the thirteen profiles at five distinct depth levels. This map demonstrates that the subsurface formation in the area's western and northern regions has exceptionally low resistivity as a result of weathering and fracturing. The majority of the survey area responds in a zone with extremely low resistivity.

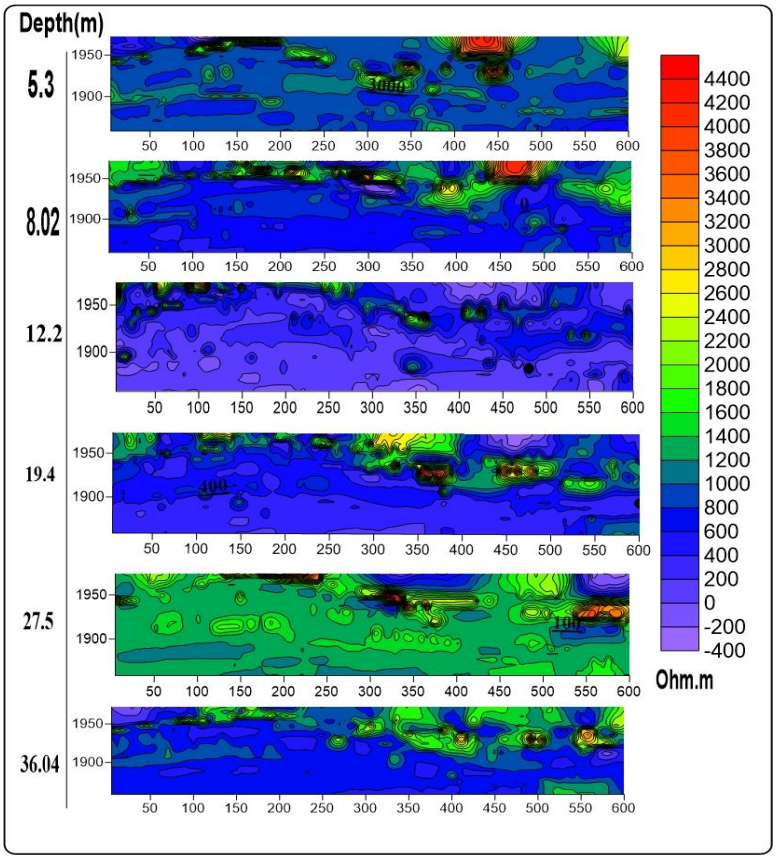

Figure 11 *Sliced-stacked plot of resistivity map as a function of dept.*

The Stacked Chargeability Map Interpretation

The chargeability sliced stacked depth was prepared from the 2D electrical chargeability dipole-dipole array data of the thirteen profiles at five different levels as shown in Figure 12. The stacked chargeability map has out lined prominent IP features on the grid. This map shows high chargeability in the southeastern part of the area. This indicates the occurrence of the minerals (rock minerals). The western and south edge of the grid was described with low chargeability value.

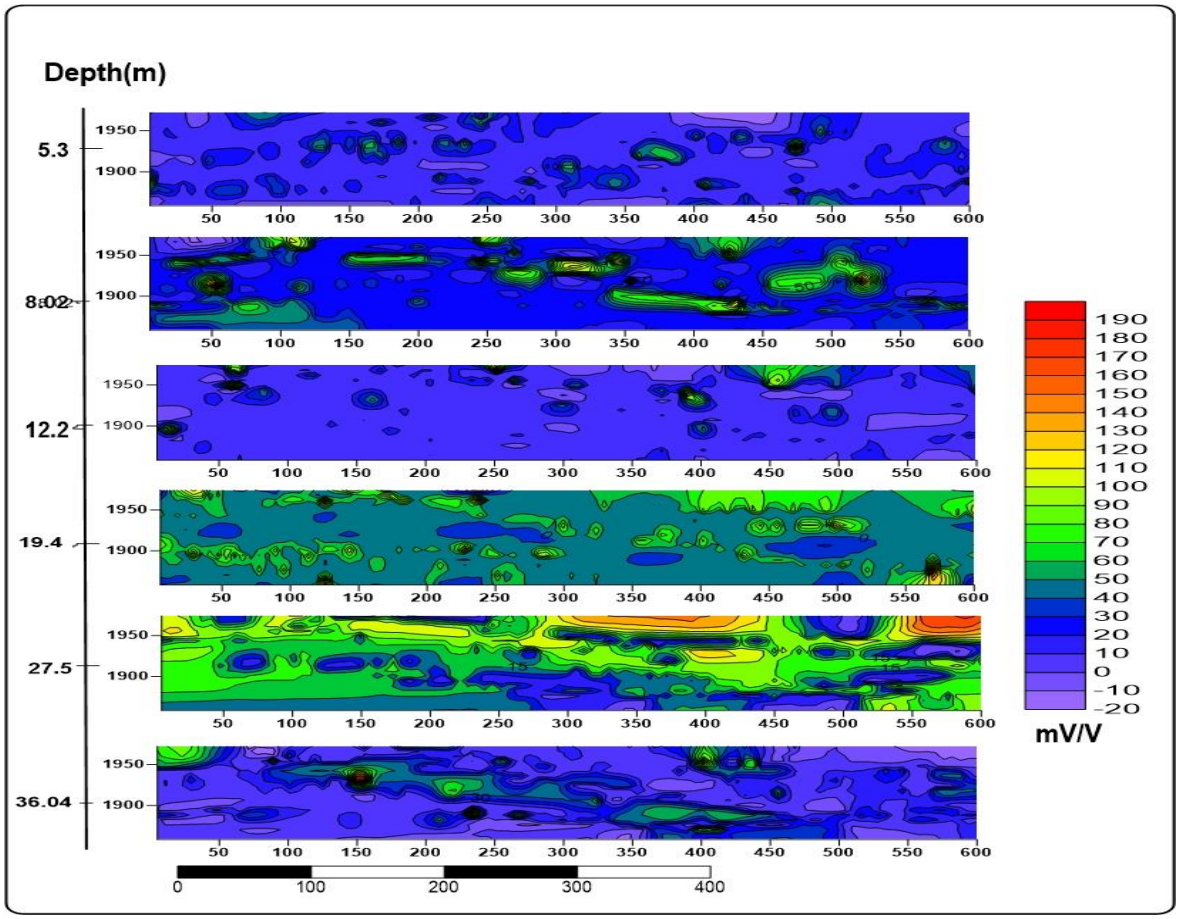

Figure 12 *Sliced-stacked plot of chargeability map as a function of depth.*

Magnetic Survey Results, Discussion and Interpretation

Total Magnetic Anomaly Maps

Figure 13's total magnetic anomaly map of the study area was divided into four sections, denoted by the distinct zones A, B, C, and D, which correspond to the various ranges of magnetic fields in the anomaly signature. Zone A represents areas with very low magnetic anomaly response because of strongly magnetised bodies from recently formed ignimbrites that are located at comparatively shallower depths. A portion of the grid area's northeastern core is covered by this zone. Zone B spans a sizable portion of the grid and exhibits low magnetic anomaly

responses that are largely influenced by geologic formations. In comparison to the other regions, Zone C patches of high magnetic signatures were found in the central, western, and eastern portions of the investigated area. It was the area where the Adere coarser-grained ultra-basic unit and the grid are associated. A significant section of the survey region, Zone D, is made up of moderately weathered fractured rock units that exhibit an intermediate magnetic anomaly response. Low magnetic anomalies were observed in the contact zones of the belt-type granitoid, meta volcanic (MV), and meta sediments (MS). This suggests that hydrothermal fluid flow through the fractures and faults has demagnetized the magnetite minerals into hematite minerals with low. magnetic response (Wilford et al., 1997). The rocks that are related with the magnetic field map are graphite schist, breccias, quartzite, and meta sediments.

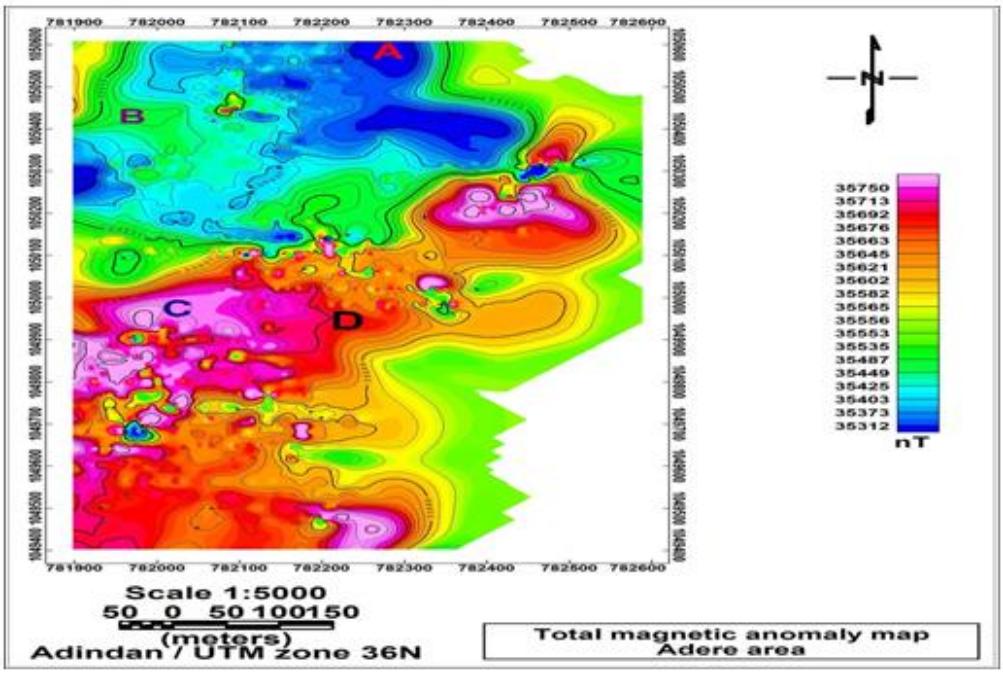

Figure 13 *Total magnetic anomaly map*

Generally, a wide quiet magnetic reief was observed over the entire metasedmentary sequence. That shows a clear geologic contact between the metasedimentary formation and the northern Adere ultra basic formation is dissemble on the map. Largely, low and broad magnetic zone was noted in the southern portion of the grid. This is due to the absence of magnetic minerals in the metasedimentary formation. Similar features were also observed in the centeral and northwestern part of the grid.

Magnetic susceptibility of rock forming minerals is generally low in intensity fractured or deformed rock units. This is because all ferromagnetic minerals are destroyed or metamorphosed in to other lithological units of lower magnetic susceptibilities. Having this idea gold occurs in susceptibility low regions. The low susceptibility metasediments, breccia,

sericte and graphite schist are associated with low magnetic susceptible principally may host gold minerilazation in the study area.

Analytical Signal Map

Analytical signal is formed through the combination of the horizontal and vertical gradient of the magnetic anomaly. The analytical signal map (Figure 14) produced maxima directly over discrete bodies and their edges. The width of the maxima is indicative of the depth of the body (MacLeod et al., 1993). The trendng lieaments are indicated on the analytical signal map revealed high contact zones which found at shallow depth. The analytical signal map shows a good correlation with the chargebilty and resitivity anomalies by bounding up with high magnetic trendig indicating the auriferous zone. The amplitude of the analytical signal gradually decreases down south as pinch and swell structure.

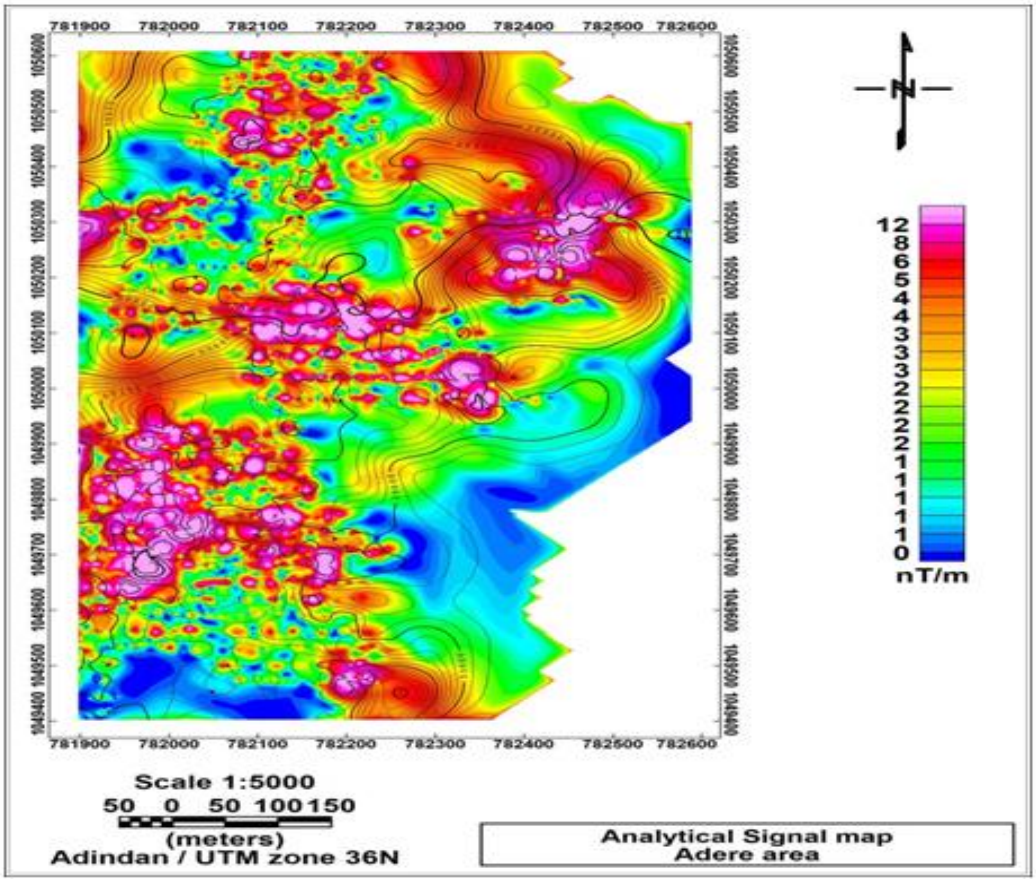

Figure 14 *Analytical Signal Ma*

First Vertical Derivative map (FVD)

The FVD map (Figure 15) helped to attenuate broad regional anomalies and enhance local, more delicate magnetic responses because of their sensitiveness to shallow magnetic source bodies and contacts. On the other hand, it is used to delineate high-frequency features more clearly, where they are shadowed by large-amplitude, low-frequency anomalies. It reveals NE-SE, NE-SW, and eastern trends in the lineaments.

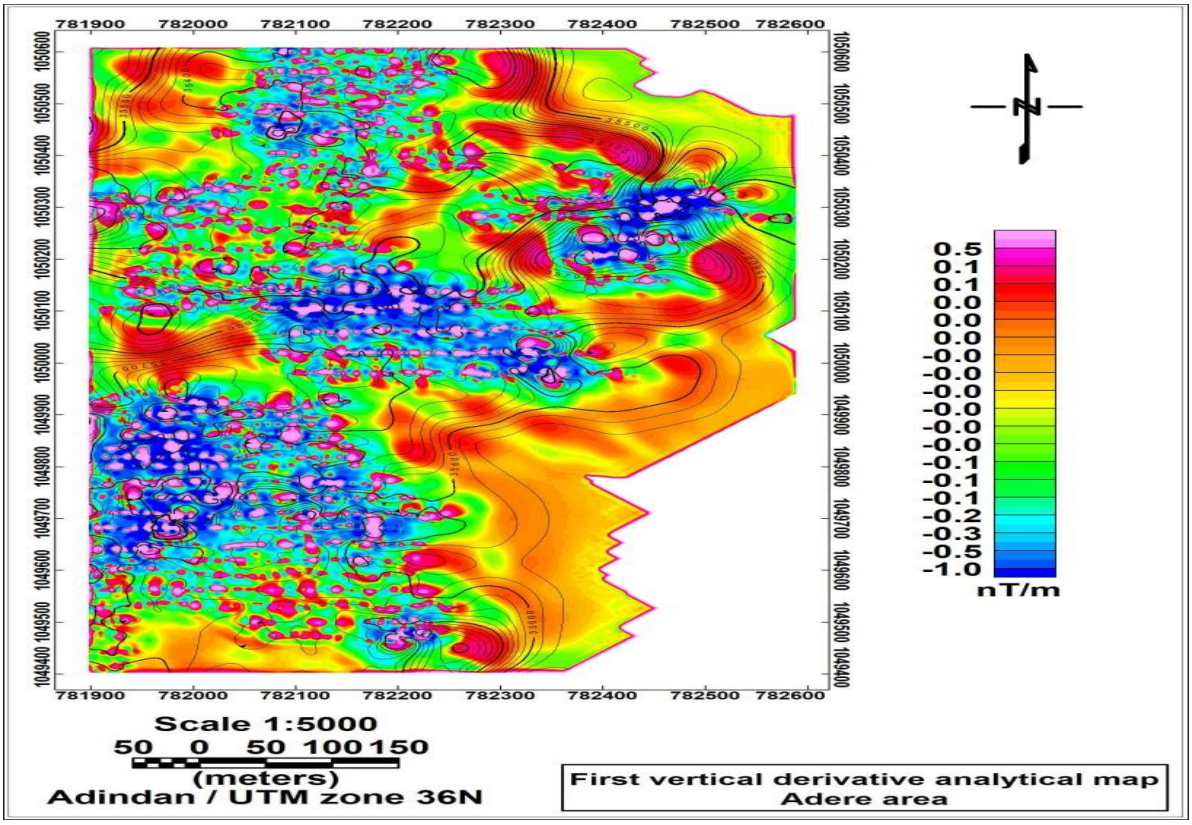

Figure 15 *First vertical derivative map of the study area*

Tilt Derivative map of the study area

The TDR map (Fegure 16) enhanced high magnetic anomalies, otherwise overshadowed by stronger structures in the area, improving subtile fabric. The NE-SW and SE-SW trending lineaments are revealed on the TDR map, which shows the metasedments and metvolcanic boundaries of the various structures on the grid.

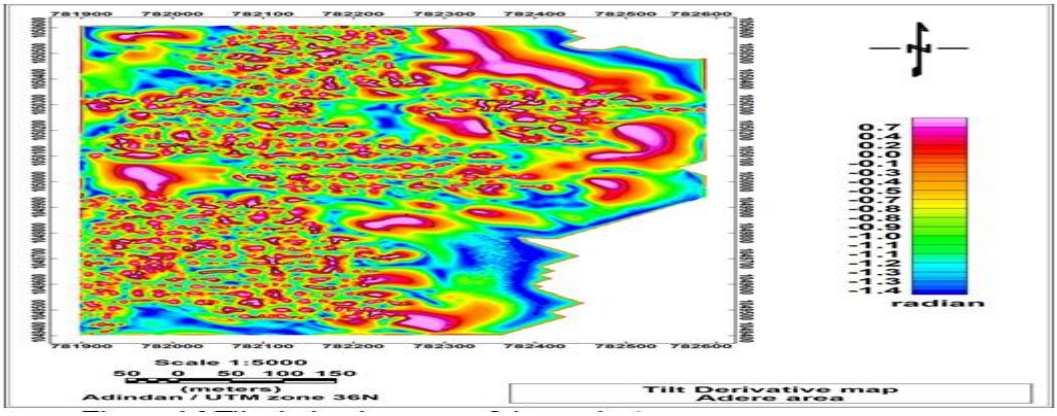

Figure 16 *Tilt derivative map of the study area*

Liniments and Representation diagram from magnetic data

Figure 17 shows a composite line segment derived from several processing methods applied to the overall magnetic field intensity data as well as line segments identified by surface geological mapping. The congrugate NE-SW and NW-SE fractures are the dominant lineaments. A major trend fitting the regional geological map was found in the NW-SW direction; other trends were found in the NW-SE direction. The channels that these structures deduced from the derivative magnetic maps were crucial for minerilization fluids. According to Moreaus et al. (1987), significant tectonic movements that took place during the pan-African Orogenic cycle resulted in the mega shear zones known as the centeral African Shear zone (CASZ), which are represented by the NE-SW trends.

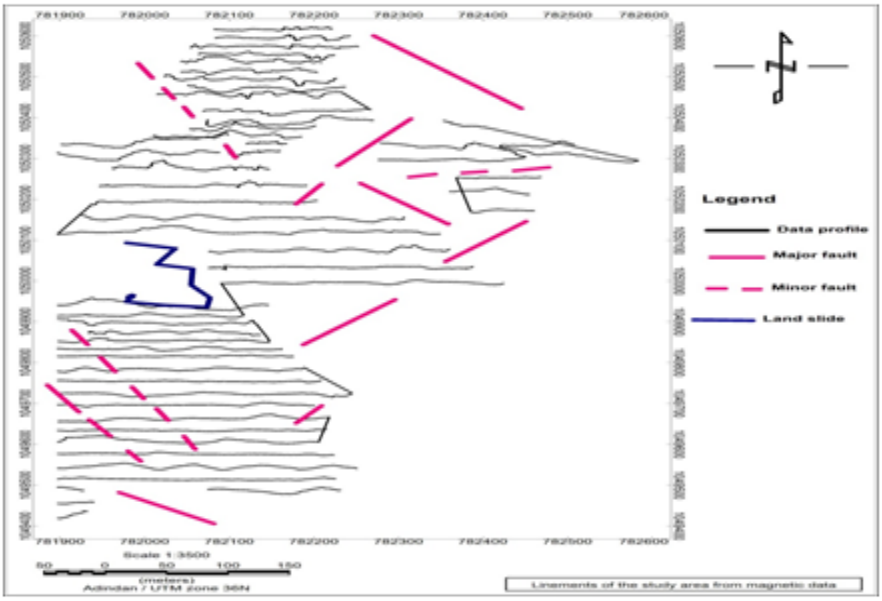

Figure 17 *Liniements and Representation diagram from magnetic data of study area*

CONCLUSIONS

An integrated geophysical investigation was conducted and identified geological signatures that could be associated with mineralization. Induced polarisation (chargeability) and resistivity maps and section plots were interpreted qualitatively and some sections quantitatively. Zones of geophysical signatures of high resistivity and medium to high chargeability indicated the prospecting zone of mineralization. These zones could be due to disseminated sulphide mineralization in hard rock or silicified formations, which could be related to economic mineral gold ccurrences. Inverted chargeability and resistivity sections of the 2D inversion model showed the anomalies to extend beyond 60 metres.

ACKNOWLEDGMENTS

The authors are deeply grateful to Wollega University for providing field facilities.

DECLARATIONS

The authors declare that there no competing interests among the researchers.

DATA AVAILABILITY STATEMENT

All data generated are available from the corresponding author upon request.

REFERENCES

Asrat, A., & Barbey, P. (2003). Petrology, geochronology and Sr–Nd isotopic geochemistry of the Konso pluton, south-western Ethiopia: implications for transition from convergence to extension in the Mozambique Belt. *International Journal of Earth Sciences*, *92*, 873-890.

Asrat, A., Barbey, P., & Gleizes, G. (2001). The Precambrian geology of Ethiopia: a review. *Africa Geoscience Review*, *8*(3/4), 271-288.

Berhe, S. M. (1990). Ophiolites in Northeast and East Africa: implications for Proterozoic crustal growth. *Journal of the Geological Society*, *147*(1), 41-57.

Getaneh, A. (2007). *Characterization of Major Subsurface Structures in Ada'a Plain Using Integrated Geophysical Survey* (Doctoral dissertation), Addis Ababa University.

Kazmin, V. (1972). Granulites in Ethiopian basement. *Nature Physical Science*, *240*(100), 90-92.

MacLeod, I. N., Jones, K., & Dai, T. F. (1993). 3-D analytic signal in the interpretation of total magnetic field data at low magnetic latitudes. *Exploration geophysics*, *24*(4), 679-688.

Sisay, M. (2008). *School of Graduate Studies Department of Earth Science* (Doctoral dissertation, Addis Ababa University.

Wilford, J. R., Bierwirth, P. E., & Craig, M. A. (1997). Application of airborne gamma-ray spectrometry in soil/regolith mapping and applied geomorphology. *AGSO Journal of Australian Geology and Geophysics*, *17*(2), 201-216.

Woldemichael, B. W., Kimura, J. I., Dunkley, D. J., Tani, K., & Ohira, H. (2010). SHRIMP U–Pb zircon geochronology and Sr–Nd isotopic systematic of the Neoproterozoic Ghimbi-Nedjo mafic to intermediate intrusions of Western Ethiopia: a record of passive margin magmatism at 855 Ma?. *International Journal of Earth Sciences*, *99*, 1773-1790.

Yada, F. A. (2017). *Petrogenesis of Plutonic Rocks from Southwest of Gimbi (Homa Area), Western Ethiopia*, (Doctoral dissertation), Addis Ababa University.

Yusefi, M. R., Hafizi, M. K., & Salari, B. (2017). Gold exploration using induced polarization and resistivity methods in Meyduk-Latala area. In *79th EAGE Conference and Exhibition 2017* (Vol. 2017, No. 1, pp. 1-3). European Association of Geoscientists & Engineers.